RESEARCH ARTICLE

Design and Implementation of a Composite Array Resistivity Data Logger for High-Resolution 2D Inversion Modeling

A.Bahrul Hidayah [1,*], M.Irsan Sadri [2], Safruddim [1], M.Rafli [1], A. Ildha Dwi Puspita [3],

[1]Geology Engineering Department, Faculty of Engineering, Hasanuddin University, South Sulawesi, Indonesia.
[2]Electrical Engineering Department, Faculty of Engineering, Hasanuddin University, South Sulawesi, Indonesia.
[3]Civil Engineering Deparment, Faculty of Engineering, Hasanuddin University, South Sulawesi, Indonesia.

* Corresponding author: bahrul.hidayah@unhas.ac.id
Tel.:+62812-1344-0863

Abstract

The use of resistivity meters to model subsurface conditions is widespread. However, commercial instruments are mostly limited to conventional configurations, such as Wenner, Schlumberger, and dipole-dipole. Moreover, we cannot modify the program on the instrument. In this study, we designed and implemented a DC resistivity meter that can potentially be developed in the future and can be used in composite array configurations. This instrument uses a half-bridge SMPS as a power supply, which is capable of generating a large power, an Arduino Uno, and several sensor modules as part of a flexible and easy-to-program control unit. We conducted laboratory and field tests, comparing two types of configurations, namely Wenner and composite arrays (dipole-dipole and gradient). We then processed the data using ResIPy software, which enables displaying complex data sets in the form of 2D cross-sections and assessing the quality of post-processing data. We obtained good data with low RMS misfit that matched the synthetic media created in laboratory testing and compared well with previous research.

Keywords: Resistivity; Array-Configuration; inversion;

1. Introduction

Subsurface geological conditions have two interrelated aspects: the potential for natural resources and the risk of geological disasters. Information on near subsurface geological conditions is required to utilize the potential of natural resources and mitigate the risk of geological disasters (Field et al., 2018). One of the most common methods is to use a geophysical instrument called a resistivity meter, which uses variations in resistivity and conductivity values in electrical resistivity tomography to generate a two-dimensional cross-sectional subsurface model (Cardarelli & Fischanger, 2006).

Exploring the nearby subsurface with the aid of physical science, technology, and concepts is known as applied geophysics. These physical fields, such as magnetic or electric fields, are invisible to human sight. The goal is to transform these detection fields into interpretable maps and graphs at this point. Matter can also be "seen" through medical imaging techniques like magnetic resonance tomography and X-rays.

Traditional geophysical techniques include exploring DC resistivity. Two electrodes are used to inject electricity into the ground, while the remaining two electrodes are used to monitor the electric potential difference. The measurements are frequently made along a line or in a specific location on the surface of the ground, and the potential differences that are subsequently seen are transformed into sounding curves or pseudosections of apparent resistivities that show the resistivity variations of subterranean rocks. (Mitchell & Oldenburg, 2023).

In any case, on the demand side, applied geophysics helps us discover and characterize aquifers. It can map soil parameters, whose subsurface composition and geometry can be determined using some supplementary information on the field of study. It can, to a certain extent, determine the location of faults, the thickness of clay layers, and more, for example, it can mark contaminated areas, find buried metal objects or outline the foundations of former settlements. (Florsch & Muhlach, 2018).

The principle of measurement using the geoelectric method is to inject a current (I) (in mA) into the earth and then measure the resulting potential difference (V) (in mV) between the two electrodes. The apparent resistance value (ρ_a) is derived from calculating the current and potential difference for each electrode distance (Loke, 2001).

Resistivity imaging is a non-invasive geophysical method widely used for subsurface exploration. One of the crucial components in resistivity imaging is the data acquisition system, which plays a crucial role in the accuracy and resolution of the imaging results (Wróbel et al., 2022). In this study, we designed a hardware system based on a microcontroller and a half-bridge switching topology power supply to implement a composite array for resistivity imaging.

The decision to use a microcontroller-based system was made to increase the flexibility and control of the data acquisition process (Hercog & Gergič, 2014). The half-bridge switching topology power supply was designed to provide high voltage and high current output (Hongxia, 2009) for deeper and better-resolved imaging. The implementation of a composite array allows for better resolution and accuracy of the imaging results (Balasco et al., 2022) .

The design and implementation of this resistivity data logger system offer several advantages over previous

systems. The microcontroller-based system provides real-time monitoring and control of the data acquisition process, allowing for better accuracy and flexibility in imaging. The half-bridge switching topology power supply provides a high voltage and high current output, resulting in better signal-to-noise ratio and deeper imaging. The implementation of a composite array allows for higher resolution imaging, especially in complex geological formations (Okpoli, 2013).

Analyses of these data enable us to find the underground resistivity anomalies or outline the subsurface geological structure. With the development of computer technology and numerical computational techniques, accurate numerical simulations of subsurface electrical field and acquiring a large amount of data in fields become possible , so that the traditional DC resistivity exploration was developed to a computerised geotomography technique, called electrical resistivity tomography, which employs a multielectrode equipment (Capa-Camacho et al., 2022).

On the apparent resistivity data, the inverse modeling technique is applied through the inversion process. Software called ResiIPy is used to perform process inversion. To translate the apparent resistivity value of the material into its actual resistivity value, the inversion method is used for complex datasets (Blanchy et al., 2020).

1.1 Earth Resistivity

An indicator of how much a material opposes the flow of electricity is its electrical resistivity. The unit of measurement for resistivity is the ohmmeter (Ω m). A material has low resistivity if electricity can easily pass through it. High resistivity refers to a material's difficulty in allowing electricity to flow through it (Heaney, 2003).

However, to determine the depth of the underground layer, we first measure the earth's resistivity. Table 1 shows how this measurement can be used to determine the depth of the underground layer.

Table 1. Soil types and their apparent soil resistivity (Nassereddine et al., 2013).

Type Of Soil Or Water	Typical Resistivity (Ω/m)	Usual Limit (Ω/m)
Sea Water	2	0,1 to 10
Clay	40	8 - 70
Ground Well and Spring Water	50	10 - 150
Clay and Sand Mix	100	4 - 300
Shale, Slate, Sandstone	120	10 - 1000
Peat, Loam, Mud	150	5 - 250
Lake and Brook Water	250	100 - 400
Sand	2000	200 - 3000
Morana Gravel	3000	40 – 10000
Ridge Gravel	15000	3000 - 30000
Solid Granite	25000	10000 – 50000
Ice	100000	10000 - 100000

The table shows that the resistivity values vary depending on the type of soil layer. Based on its resistivity value, this value is then utilized as a reference for underground mapping.

1.2 Electrical Resistivity Tomography

The two-Dimensional Electrical Resistivity Tomography (2D ERT) technology is particularly capable of resolving subsurface structures in fact, constructing a 2D representation of ground using two current electrodes and measuring the potential drop (V) across the other two electrodes (Thapa, 2020). The measured voltage drop is directly proportional to the electrical resistivity, which can be related to the medium's distinguishing features as follows:

$$\rho = K\,\Delta V/I \tag{1}$$

Where I represent Current (Ampere), ΔV represents potential difference (V), K represents the geometric Factor (meter) and Ω represents resistivity value (Ohm.m).

Using a large number of resistivity measurements from electrodes arranged in any geometric form, the ERT method determines the subsurface distribution of electrical resistivity. ERT uses four electrodes to minimize the impact of contact resistance at the interface between the soil pore water and the electrode. A known current is driven through two electrodes, and the potential difference on the other two electrodes is monitored (Daily et al., 2005).

All conceivable linearly independent combinations from an array of electrodes are employed to obtain the high number of separate impedance measurements required for tomographic inversion. Various configurations can be used to generate these pairings. A Wenner Alpha measurement scheme is a prominent approach for field measurement.
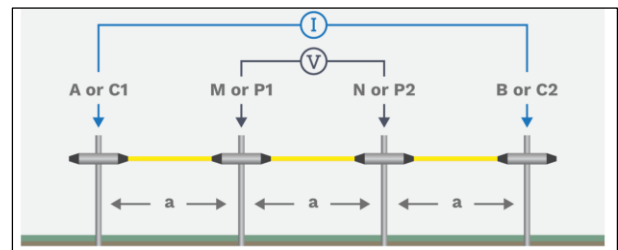
Fig 1. Wenner Alpha Array Configuration (Aktarakçi, 2017).
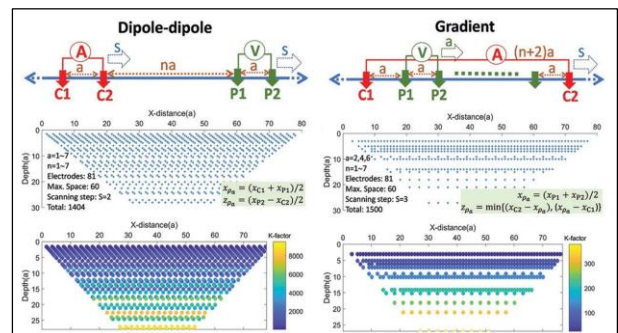
Fig 2. Dipole-dipole Array Configuration (Oyeyemi et al., 2022).

To obtain apparent resistivity in the field, many electrode sets were developed in the traditional DC resistivity exploration. In principle, ERT requires high data density and good earth surface coverage for high-resolution subsurface target imagery. Data retrieval in this study carried out experiments using 2 array configurations, namely the 'conventional' Wenner

configuration and the composite configuration of a combination of dipole-dipole and gradient configurations

1.3 Inversion Process Optimization

Inverse methods must be used to convert geoelectrical measurements into geoelectrical attributes. These techniques seek to identify the geoelectrical parameter distribution that is most compatible with measured data. To do this, the mismatch between the set of readings from four electrodes and the anticipated response from a geoelectrical model must be minimized.

ResIPy is a program for geophysical data analysis, modeling, and inversion that makes the issue simple and gives users complete control over complex modeling and inversion parameters through a clear graphical user interface. ResIPy offers a platform for interdisciplinary projects where trustworthy outcomes are provided through a nonlinear user interface that is simple to use. ResIPy is perfect for educational uses as it enables modeling and inversion of 2D and 3D resistivity and IP data. While the majority of inversion algorithms and software on the market can perform simple data filtering, ResIPy offers a comprehensive data-cleaning technique. Both the GUI and the API have been used to successfully implement ResIPy in a variety of modeling and field applications (Blanchy et al, 2020).

2. Instrument Design

2.1 Hardware Design

The initial process of this tool is through a safety device in the form of a voltage protection relay, then the input voltage which was previously 12V is increased to approximately 400V using a DC-DC boost converter.

The increased input voltage is then measured, if no current is detected, we can take measurements. As many as 24 electrodes will be plugged into the ground, where the electrode configuration will be changed through the switch box. Then the ampere meter and volt meter will detect the value of voltage and current. We can monitor the voltage and current values of the electrodes via the LCD, and the data will automatically be recorded to the SD Card.
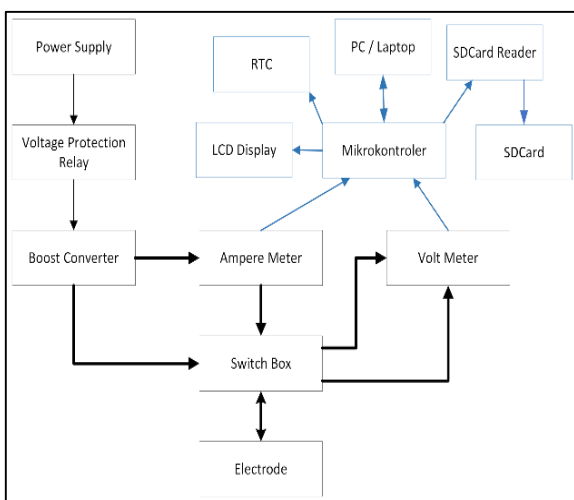
Fig 3. Resistivity Meter Data-Logger Design Schematic

Laptops are used to enter data display programs on the LCD screen and record data on the SD Card into the microcontroller. Where the microcontroller here plays an important role as the brain of the Arduino circuits. Fig 3. is a rough idea of how this tool will be made

2.2 Power Supply

Switch mode DC power sources frequently employ DC/DC converters. The output voltage regulation of the DC/DC converter is accomplished from an energy perspective by continuously changing the energy absorbed from the source and that injected into the load, which is in turn regulated by the relative durations of the absorption and injection intervals. A switching cycle is made up of these two fundamental energy absorption and injection processes (Hasaneen & Elbaset Mohammed, 2008).

Half-bridge switch-mode power supplies (SMPS) are commonly used in high voltage and high current applications due to their capability to handle high power levels while being cost-effective.

According to a study by H. Yang et al. (2017), a half-bridge SMPS is suitable for high voltage applications due to its ability to step up voltage levels efficiently. The authors demonstrated that a half-bridge SMPS can be designed to operate at high voltages up to 1 kV with an efficiency of over 90%.

In terms of high current applications, a half-bridge SMPS can also be designed to handle high current levels. A study by R. Devi et al. (2020) demonstrated the design and implementation of a half-bridge SMPS capable of delivering high current up to 10 A. The authors also showed that the use of a half-bridge SMPS resulted in lower cost and better efficiency compared to a full-bridge SMPS.

Overall, a half-bridge SMPS is capable of handling high voltage and high current applications while being cost-effective. The design and implementation of a half-bridge SMPS should take into consideration the specific requirements of the application to optimize its performance.

In DC resistivity measurements, the use of a high voltage and high current power supply can result in better signal-to-noise ratio (SNR) and lower root mean square (RMS) misfit.

According to a study by R. Kumar et al. (2016), high voltage and high current can help to overcome the limitations of low SNR and high RMS misfit in DC resistivity measurements. The authors found that increasing the current and voltage in the measurement system can improve the quality of the acquired data and reduce the uncertainty in the results (Sirota et al., 2022).

Another study also supported the use of high voltage and high current power supplies in DC resistivity measurements. The authors demonstrated that using a high voltage and high current power supply can improve the accuracy and precision of the measurements, particularly in low-resistivity regions (Balasco et al., 2022).

as in the schematic diagram in fig 4. two transistors are used in the half-bridge topology of a DC-DC converter to start switching activity, which sends current pulses to a load. This DC-DC converter topology offers pulses that can be smoothed to a nominal DC power value in addition to rectification and smoothing with a capacitor bank. This topology can be isolated, allowing it to produce high voltages when linked in series from multiple boards, with output power being coupled through a transformer or optocoupler. If the gate driver circuit is an integrated circuit, isolation may be applied within it by junction

isolation. Transformer coupling may also be used in non-isolated topologies to increase or decrease the output voltage (Fathy et al., 2006).
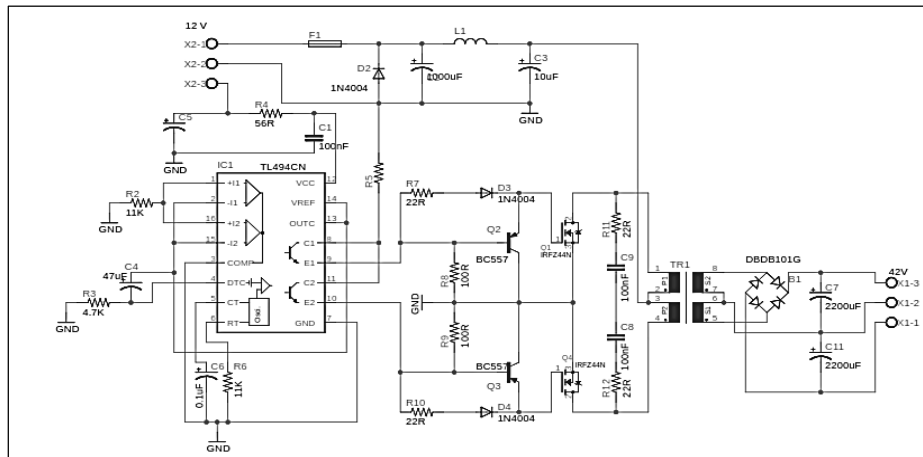
Fig 4. Half-Bridge DC-DC Boost Converter Schematic Circuit

Due to their simplicity, flyback and forward topologies are frequently used in isolated DC-DC converters for low Power Supply Units (PSU) with less than 1 kW. In contrast to the Flyback converter, the forward converter's high-frequency transformer does not store energy, making it more suitable for applications requiring high output current (Ezra et al., 2022).

2.3 Switch Box

Each new measurement necessitated the movement of all four electrodes. Single-channel imaging equipment that can switch the current injection and potential reading locations between a restricted number of electrodes became commercially accessible in the 1990s. Today, more advanced instruments use several channels to address enormous numbers of electrodes (Binley & Slater, 2020). This was the main idea of this manual switch box.

The development of multi-electrode instrumentation in the late 1980s stimulated parallel advances in algorithms for 2D imaging of resistivity. By adjusting the relationship between the voltmeter (P1 and P2) and the ammeter (C1 and C2) on the switch box that is connected to the electrode as needed, researchers can perform a variety of electrode array configurations with only one implant of electrodes.
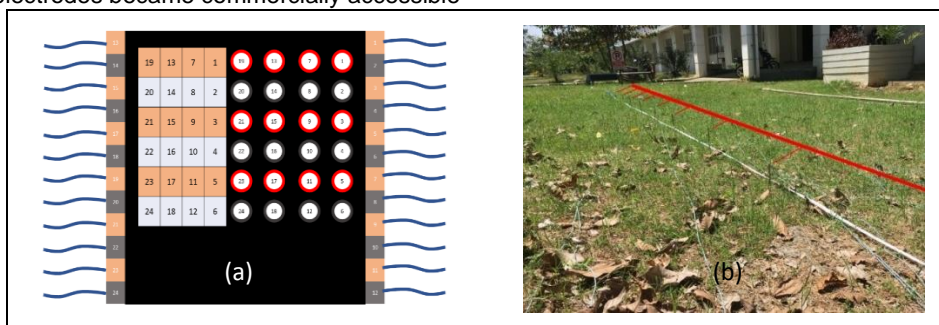
Fig. 5. (a) Switch Box Design; (b) Electrode Distribution based on Switch Box
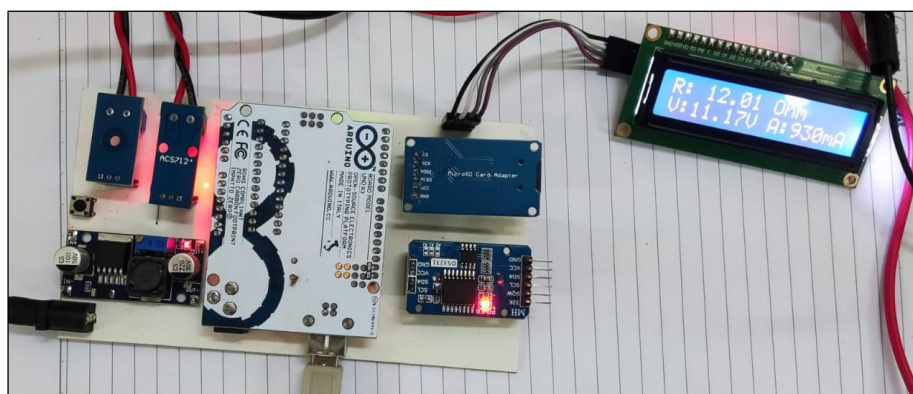
Fig 6. The voltage sensor, current sensor, RTC, data storage, voltage reference, and LCD screen are all connected and work simultaneously and that is controlled by the microcontroller.

2.4 Microcontroller

An embedded computer control application-specific single-chip computer is known as a microcontroller. These devices are relatively inexpensive and very simple to utilize in digital control applications. The majority of microcontrollers come with the integrated circuitry required for computer control applications. For instance, a microcontroller might include A/D converters to enable the sampling of external signals. Additionally, they contain parallel input-output connections that allow the microcontroller to read or produce digital data.(Ibrahim, 2006).

The primary brain of the programmed components is the microcontroller. The microcontroller in this case is set up to read data from the voltmeter, ammeter, and real-time clock and show it on the LCD screen while concurrently writing the data to the SDCard (RTC). The microcontroller component can be seen in fig 6.

2.5 Voltage Protection Relay

The following schematic circuit diagram in fig 7 is intended as protection in the form of overvoltage and Undervoltage protection which works in conditions when the input voltage is more than 14.5V or less than 11.6V. When the overvoltage is above 14.5V, the comparator in the circuit will cut off the NO connection to the relay from the power source, as well as when the voltage is below 11.6V.
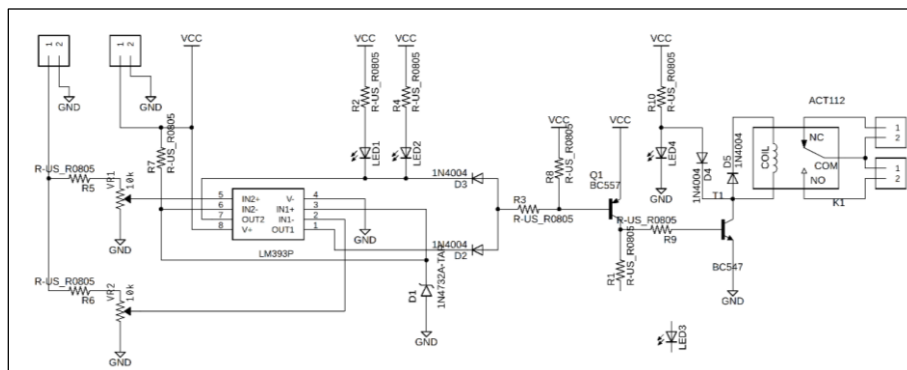
Fig 7. Voltage Protection Module Schematic Circuit

The comparator will disconnect the NO from the relay from the power source. This protection is intended to protect the boost converter when the voltage is excessive and protect the power source (battery) when it is at a voltage of less than 11.6V. The opposing activities that create overvoltage can result in Undervoltage. Undervoltage conditions will result in the potential for electronic device failure, and a decrease in the reactive power output from capacitor banks. (Kotb et al., 2018).

2.6 Performance Testing Setup

Laboratory tests are carried out after the tools have been successfully assembled and meet the proper requirements including controlled test media for laboratory tests in fig 9. The electrodes used in this experiment are made of stainless steel. Because stainless steel electrodes are typical metal electrode that is relatively inert and affordable. (Binley et al., 1996).

This test was carried out in the Hasanuddin University campus environment, and fig 5b and fig 8. And shows how the electrode and the resistivity meter are set up in field tests. where data was obtained twice in this test utilizing different electrode setups We will then compare the measurement data from the Wenner alpha configuration with those from the gradient dipole arrangement.

Fig. 8. Field testing setup after all components of the resistivity meter data logger are assembled
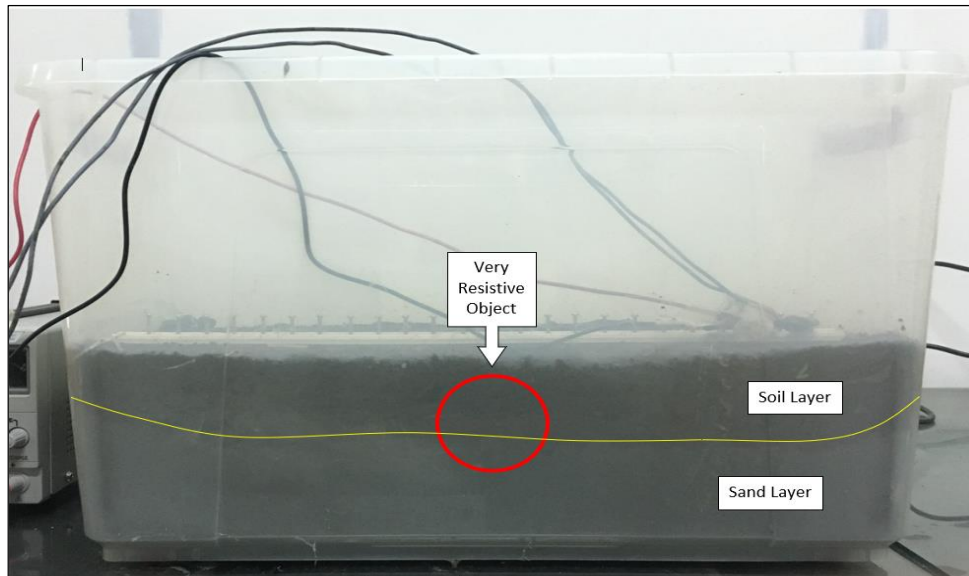
Fig. 9. Synthetic media consisting of layers of soil, sand, and high resistivity object (plastic bottle)

3. Result

In this study, we compared the results of similar previous studies by comparing the quality of the data produced by looking at the percentage of RMS misfit in the 2D inversion results also compared the performance of a tool in measuring resistivity parameters using two electrode configurations. Additionally, we put the tool to the test by determining whether its output accurately describes the situation of the controlled test material utilized in laboratory testing. In the test medium, an object with high resistivity was placed in the middle of two layers of dirt and sand. Following laboratory testing, the tool was also tested in the field using two distinct electrode configurations.

RMS misfit is a commonly used parameter for evaluating the accuracy of 2D resistivity models, as mentioned by Olayinka & Yaramanci, 2000. The root-mean-square misfit is calculated by taking the square root of the average of the squared differences between the observed and modeled resistivity values. A low RMS misfit value is generally considered to be acceptable for 2D resistivity models, while a high RMS misfit value indicates a poor fit between the observed and modeled resistivity values.

Uhlemann et al., 2018 conducted a geophysical investigation using electrical resistivity tomography (ERT) as a tool to guide ornamental stone extraction. The researchers shows the inverted resistivity model, for which the relative root-mean-squared (RMS)misfit between modelled and measured data was RMS = 2.1%. For visualizing and interpreting theresistivity models, all cells with sensitivities $<5\times10^{-3}$ were removed from the model. Using this approach, the depth of investigation can be approximated to be about 10 m. The study identified factors that affected the RMS misfit values, including variations in the electrode configurations, measurement errors, and subsurface heterogeneity.

Abdullah et al., 2018 assessing the reliability and performance of optimized and conventional resistivity arrays for shallow subsurface investigations. The researchers reported an RMS misfit value of 1.36% -

6.9% for the study. The study identified several factors that influenced the RMS misfit values, including the accuracy of the electrode placement, the presence of noise in the data

Dahlin & Zhou, 2006 conducted research two-dimensional resistivity imaging using composite arrays, Wenner and dipole-dipole electrode arrays was carried out at two field sites in Sweden and one in Nicaragua, with the objective of confirming the practical applicability of results obtained with numerical modelling. The results support earlier numerical modelling studies that concluded that the composite array, using multiple current electrode combinations, has resolution as good as or better than the commonly used Wenner array. The array behaved well in terms of sensitivity to noise at the test sites, and the results obtained generally agree with dipole-dipole array results, although the latter at two of the sites gave resistivities that differed significantly from the other arrays in the deeper parts of the inverted model

Drawing on prior research, laboratory experiments were conducted to evaluate the efficacy of the instrument, we proceeded to conduct measurements in the field using the Wenner Alpha and dipole-dipole composite array electrode configurations. The resistivity meters were used to take measurements with both electrode configurations. These measurements were then further processed with ResIPy, an open-source software, which produced a temporary resistivity value. The data were iterated further until a fairly low RMS value was achieved. The initial design of the test medium for these measurements is shown in fig. 9.

3.1 Laboratory test (Dipole – dipole gradient configuration)

The apparent resistivity value in the experiment is shown in the graphic below (Fig. 10) using a Composite configuration and the data captured by the device that has been made. Some points appear empty because that data has a high transfer resistance rate and may be considered invalid, the data is then removed and left blank so that the software algorithm can interpolate it automatically later.
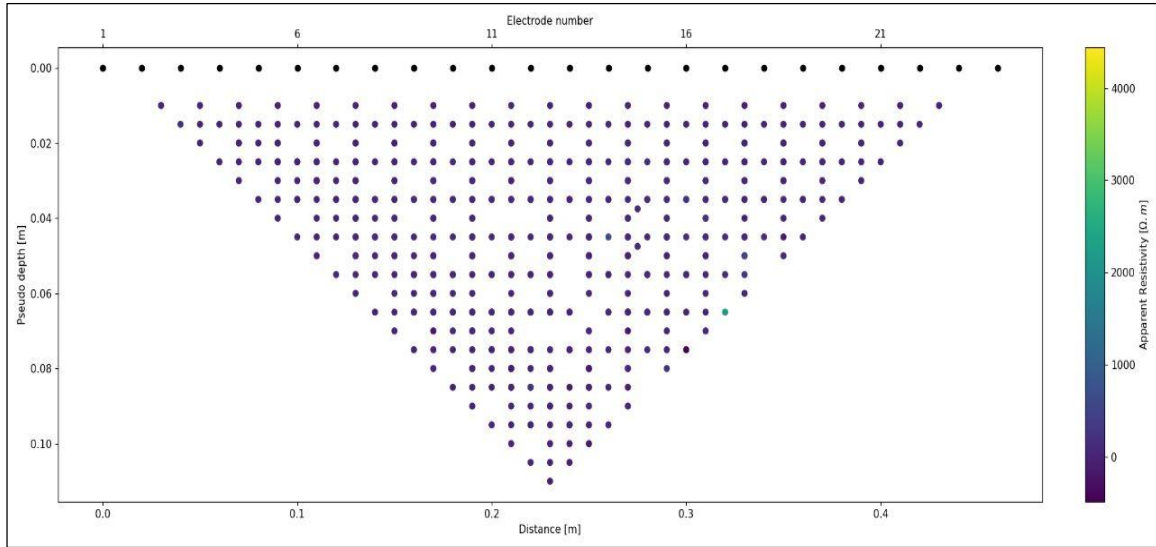
Fig. 10 Laboratory test: Composite Array Configuration Apparent Resistivity
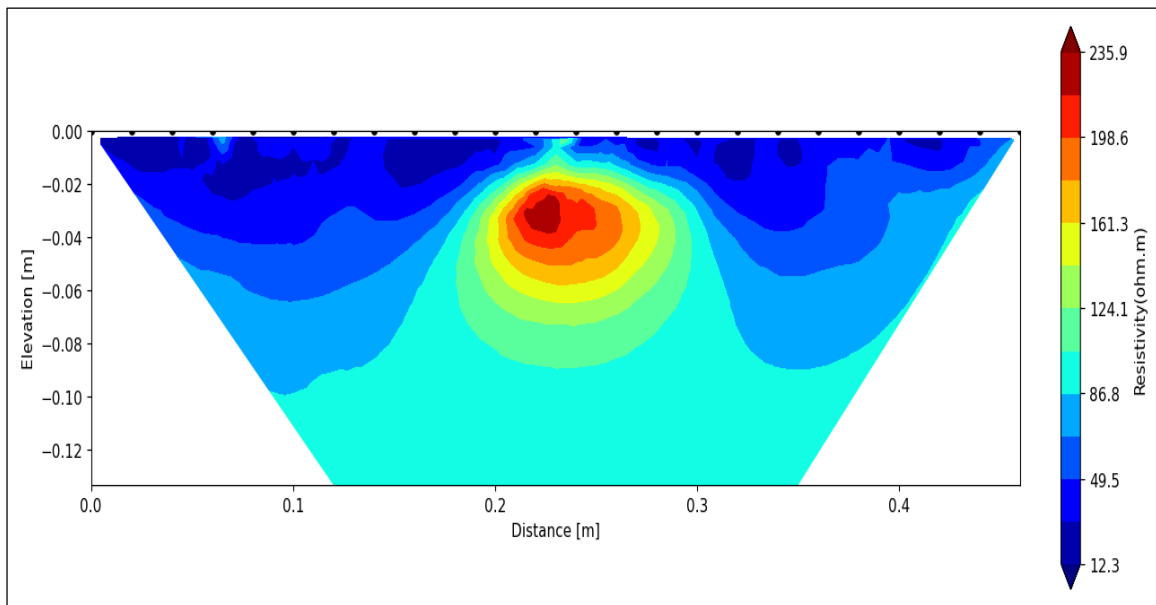
Fig. 11 Final Result: Composite Two-Dimensional Resistivity Imaging

After importing the data and getting a pseudo resistivity value, it will be further processed to get the original resistivity value by examining the geometric factor and doing several iterations to reduce the RMS (root-mean-square) error value in the data obtained. Two-Dimensional Resistivity Imaging shows a fairly clear picture of layers and shapes of different resistivity values on the test media, where the coarse sand mixed with soil at the bottom of the media shows a resistivity range of 60-236 Ohm.m, in the upper layer which is consisting of soil mixed with clay showing resistivity values in the range <12 - 87 Ohm.m while the round resistive object in the center of the test medium has a resistivity value of <237 Ohm.m, represented in fig. 10 and fig 11.

3.2. Field measurement test: (Field test, Apparent Resistivity)

The fig.12 and fig 13. depicts the apparent resistivity value derived from the measurement data, which can

be viewed as a dot in the image representing the datum. Where the data is recorded by the tool, the distribution of the dots in the image is determined by the configuration of the electrodes.

As a result, the number of points in the image denotes that the data obtained by these measurements correspond to the number of dots in the image. Fig. 12 (composite array) and Fig. 13 (Wenner alpha configuration) show that the amount of data recorded from the two configurations differs significantly.

In Fig. 12 (Composite configuration) the apparent resistivity values are in the range of 120000 Ohm m to -20000 Ohm m and in the image, it can be seen that the data has a fairly high density.

In Fig.13 (Wenner Alpha Configuration), the apparent resistivity values are in the range of 2500 Ohm m to -17500 Ohm m and the data density is quite far compared to the data density from the composite configuration.
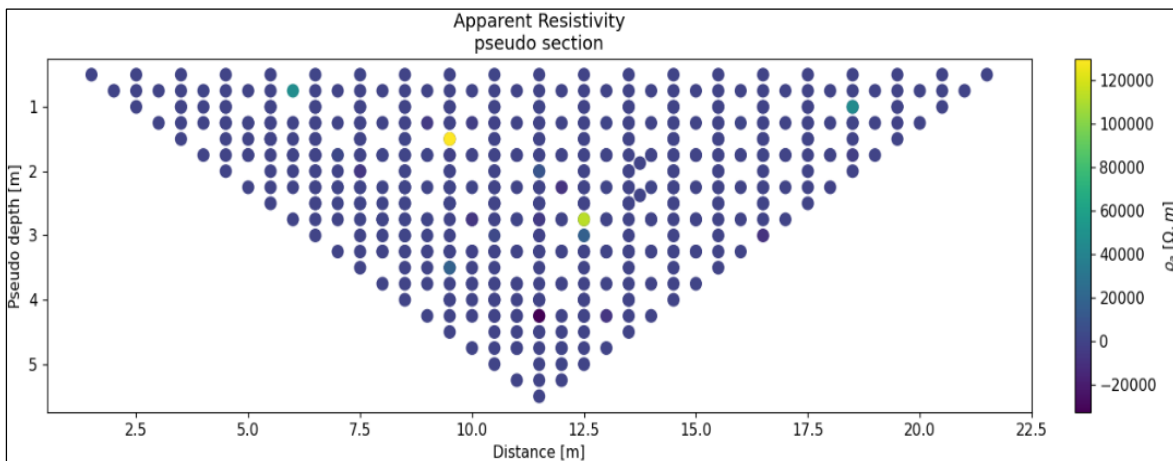
Fig. 12 Field test: Apparent Resistivity using composite array dipole-dipole gradient.
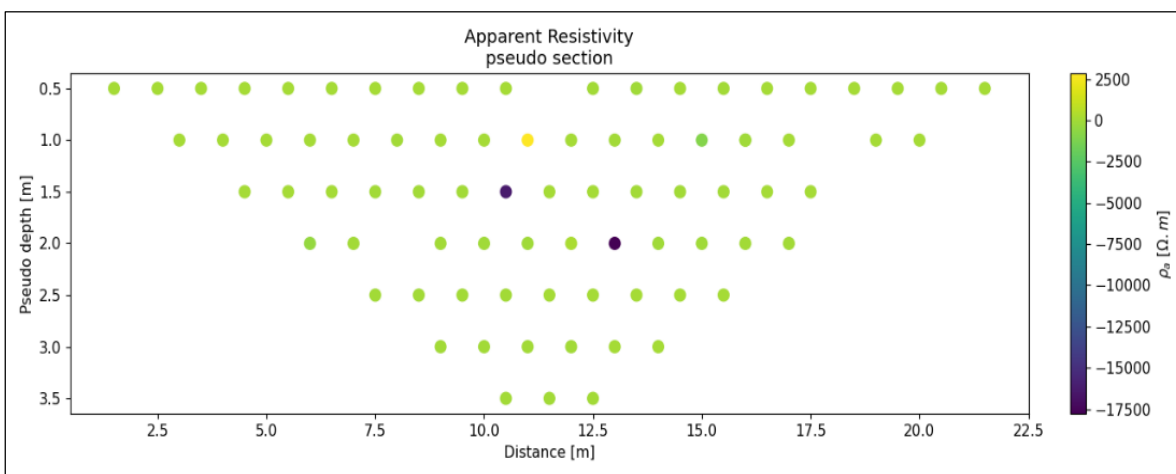
Fig. 13 Field test: Apparent Resistivity using wenner alpha array configuration.

3.2.1 Field Test, Iteration & Root-mean-square (RMS) error of inversion results

Fig. 14 and fig. 15 show the relationship between iterations and the RMS misfit value resulting from this measurement. This iteration is one stage of the underground depiction interpretation process, where the inversion process requires iterations to reduce the RMS error value from the measurement results. It can be seen that the two configurations below have been carried out with several iterations to reduce the RMS error value. In Figure 15 (Dipole-dipole configuration) the initial RMS error value is 21.12% and after six iterations, the final RMS error value is 1%, While in Figure 16 (Wenner Alpha Configuration), it can be seen in the graph that the initial RMS error value is quite high at 42.46%. After ten iterations, the RMS error value decreased to the level of 1.32%.
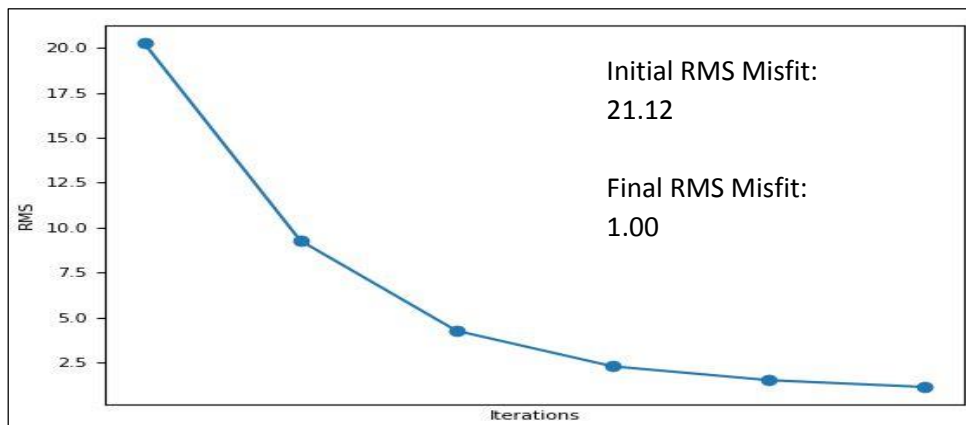
Fig. 14 Field Test: Iteration & RMS Value (Dipole-dipole gradient)
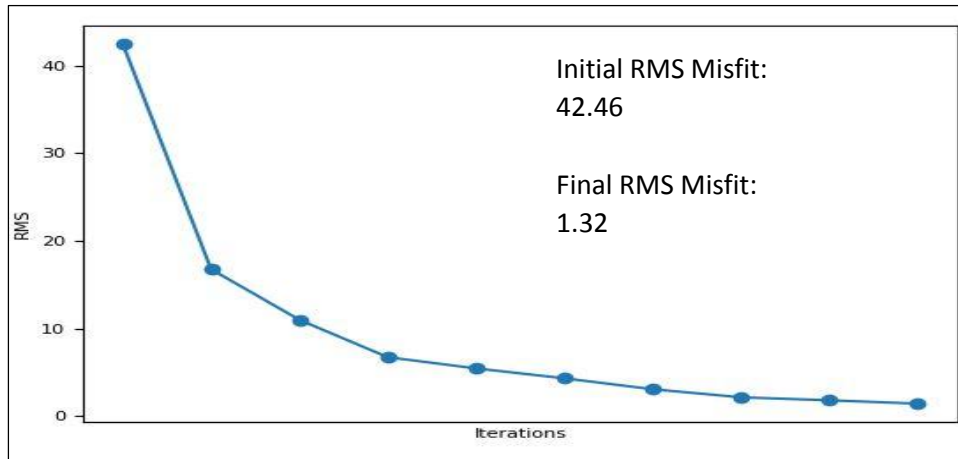
Fig. 15 Field Test: Iteration & RMS Value (Wenner Alpha)

3.2.2 Field Test, Normalized Error

Fig.16 and fig. 17 below illustrate the spread of data errors where the data has gone through the inversion process including iteration.

In Fig. 16 which uses a gradient dipole configuration, it can be seen that the data error spread is in the range of 1.5% to - 1.5%. While in Figure 17 which illustrates the spread of data errors using the Wenner Alpha configuration, it can be seen that the error value is past 2% but does not exceed the specified fault tolerance limit.

This is most likely influenced by the amount of data that has a significant difference between the two types of electrode configurations. Where interpolation or depiction can be easier or more precise when you have a lot of data.
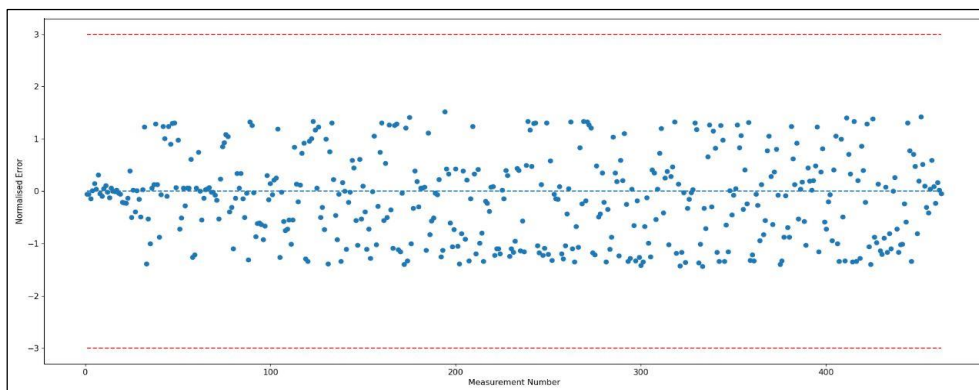
Fig. 16 Field Test: Normalized Error (Dipole-dipole gradient)
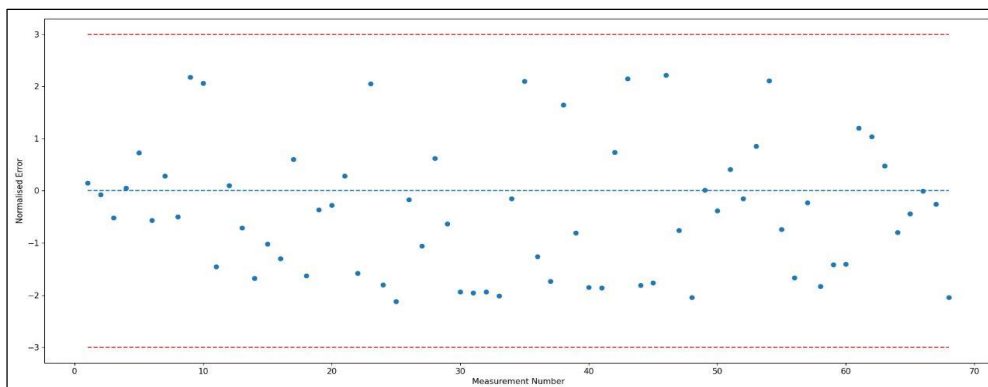
Fig. 17 Field Test: Normalized Error (Wenner Alpha)

3.2.3 Field Test, Final Result

The two images below are obtained after going through several stages of the process to get the results of the depiction based on the data obtained by the tool.

It can be seen that the two images below (Fig. 18 and Fig.19) are almost identical to each other. This can be a consideration that the results given are appropriate because after doing two measurements the results are still almost the same.

In Fig. 18 with a composite electrode configuration, it can be seen that the resistivity value recorded is more detailed or has a fairly high-resolution value, while Figure 19 does produce almost the same image but the resistivity value recorded produces a fairly rough image in the mapping.
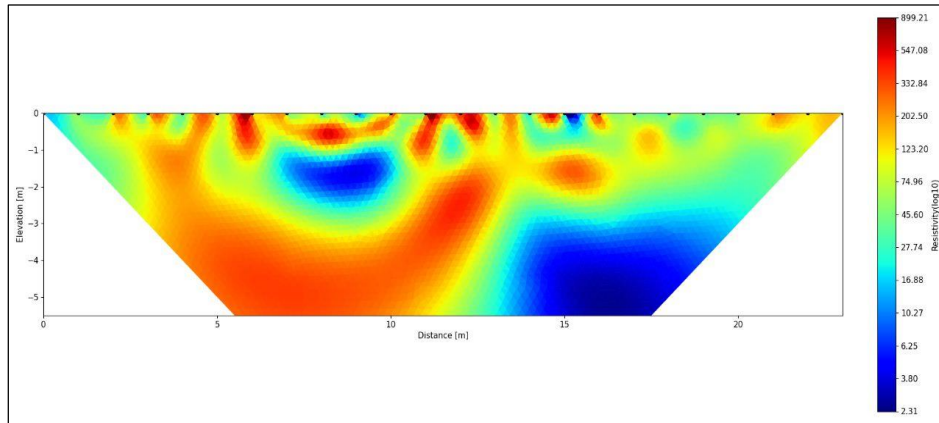
Fig. 18 Field test: Final Result (Composite Array Configuration)
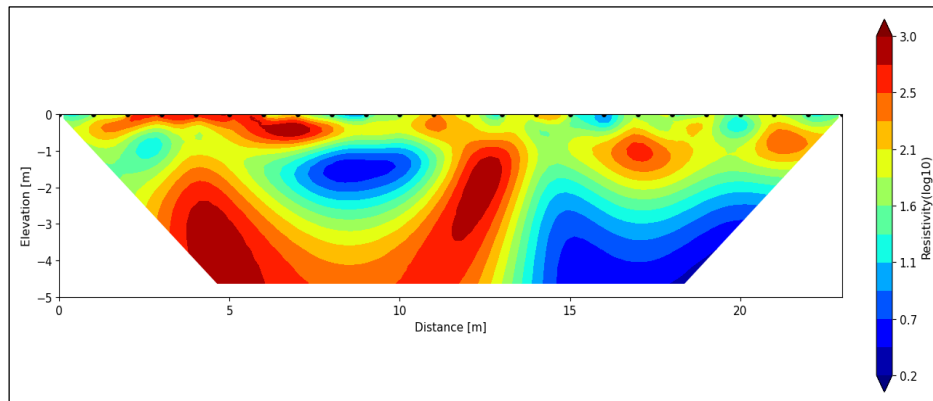
Fig. 19 Field test: Final Result (Wenner Alpha Configuration)

4. Conclusions

The laboratory test results are satisfactory, the resistivity meter test results show the performance as expected, getting a relatively small RMS misfit value when compared to existing research.. The resulting two-dimensional profile is quite good in describing the test media that have been made.

Voltage and current measurements performed with this tool produce good results because the data that obtained is also still within the error tolerance limit of +/- 3%, the theoretical test may be declared to be successful, allowing the instruments to be tested in the field. This was based on (Binley et al., 1995), where the values of error should be generally between -3 and +3 percent, with no obvious patterns, if the zero mean uncorrelated error assumptions are true.

When we ran the test on the field with the composite configuration, we got a +/- 1.5% normalized error. Following that, we performed a second measurement using the Wenner Alpha configuration, with an error value of +/- 2.5%.

This could be related to the enormous amount of data that differs between the two configurations, based on the data generated by the Wenner Alpha configuration, which

has a greater error value than the dipole-dipole configuration. Whereas the wenner alpha configuration generates approximately 80 datums, the Dipole arrangement generates approximately 520 datums. The measurement findings demonstrate that the Wenner Alpha configuration, which uses significantly less data than the dipole-dipole configuration, can depict the lateral split of the field more clearly. However, the dipole-dipole configuration measurement outcomes offer processed data with a greater resolution or make the shape of the item more obvious.

Acknowledgments

References

Abdullah, F. M., Loke, M. H., Nawawi, M., & Abdullah, K. (2018). Assessing the reliability and performance of

optimized and conventional resistivity arrays for shallow subsurface investigations. *Journal of Applied Geophysics*, *155*, 237–245. https://doi.org/10.1016/j.jappgeo.2018.06.018

Aktarakçi, H. (2017, June 10). *Wenner Array: Electrical Resistivity Methods, Part 1.* https://www.agiusa.com/wenner-array

Balasco, M., Lapenna, V., Rizzo, E., & Telesca, L. (2022). Deep Electrical Resistivity Tomography for Geophysical Investigations: The State of the Art and Future Directions. *Geosciences*, *12*(12), 438. https://doi.org/10.3390/geosciences12120438

Binley, A., Ramirez, A., & Daily, W. (1995). *Regularised Image Reconstruction of Noisy Electrical Resistance Tomography Data.*

Binley, A., Shaw, B., & Henry-Poulter, S. (1996). Flow pathways in porous media: electrical resistance tomography and dye staining image verification. *Measurement Science and Technology*, *7*(3), 384–390. https://doi.org/10.1088/0957-0233/7/3/020

Binley, A., & Slater, L. (2020). *Resistivity and Induced Polarization Theory and Applications to the Near-Surface Earth*. https://doi.org/10.1017/9781108685955

Blanchy, G., Saneiyan, S., Boyd, J., McLachlan, P., & Binley, A. (2020). ResIPy, an intuitive open source software for complex geoelectrical inversion/modeling. *Computers & Geosciences*, *137*, 104423. https://doi.org/https://doi.org/10.1016/j.cageo.2020.104423

Capa-Camacho, X., Martínez-Pagán, P., Martínez-Segura, M. A., Gabarrón, M., & Faz, Á. (2022). Electrical resistivity tomography (ERT) and geochemical analysis dataset to delimit subsurface affected areas by livestock pig slurry ponds. *Data in Brief*, *45*.

Cardarelli, E., & Fischanger, F. (2006). 2D data modelling by electrical resistivity tomography for complex subsurface geology. *Geophysical Prospecting*, *54*(2), 121–133. https://doi.org/10.1111/j.1365-2478.2006.00522.x

Dahlin, T., & Zhou, B. (2006). Multiple-gradient array measurements for multichannel 2D resistivity imaging. *Near Surface Geophysics*, *4*(2), 113–123. https://doi.org/10.3997/1873-0604.2005037

Daily, W., Ramirez, A., Binley, A., & LaBrecque, D. (2005). 17. Electrical Resistance Tomography—Theory and Practice. In *Near-Surface Geophysics* (pp. 525–550). Society of Exploration Geophysicists. https://doi.org/10.1190/1.9781560801719.ch17

Ezra, N., Werner, T., & Long, T. (2022). Dual Voltage Forward Topology for High Efficiency at Universal Mains. *Electronics*, *11*(7), 1009. https://doi.org/10.3390/electronics11071009

Fathy, K., Lee, H. W., Mishima, T., & Nakaoka, M. (2006). Boost-Half Bridge Single Power Stage PWM DC-DC Converter for Small Scale Fuel Cell Stack. *2006 IEEE International Power and Energy Conference*, 426–431. https://doi.org/10.1109/PECON.2006.346689

Field, B., Barton, B., Funnell, R., Higgs, K., Nicol, A., & Seebeck, H. (2018). Managing potential interactions of subsurface resources. *Proceedings of the Institution of Mechanical Engineers, Part A: Journal of Power and Energy*, *232*(1), 6–11. https://doi.org/10.1177/0957650917717628

Florsch, N., & Muhlach, F. (2018). Direct Current Electrical Methods. In *Everyday Applied Geophysics 1* (pp. 27–103). Elsevier. https://doi.org/10.1016/B978-1-78548-199-4.50002-7

Hasaneen, B. M., & Elbaset Mohammed, A. A. (2008). Design and simulation of DC/DC boost converter. *2008 12th International Middle-East Power System Conference*, 335–340. https://doi.org/10.1109/MEPCON.2008.4562340

Heaney, M. (2003). *Electrical Conductivity and Resistivity* (pp. 7–1 to 7).

Hercog, D., & Gergič, B. (2014). A Flexible Microcontroller-Based Data Acquisition Device. *Sensors*, *14*(6), 9755–9775. https://doi.org/10.3390/s140609755

Hongxia, W. (2009). The Research of Half-bridge DC/DC Converter Based on DSP. *2009 Third International Symposium on Intelligent Information Technology Application*, 545–548. https://doi.org/10.1109/IITA.2009.51

Ibrahim, D. (2006). Microcontroller Project Development. In *Microcontroller Based Applied Digital Control* (pp. 119–130). https://doi.org/https://doi.org/10.1002/0470863374.ch5

Kotb, M., El-Saadawi, M., & El-Desouky, E. (2018). Design of Over/Under Voltage Protection Relay using Arduino Uno for FREEDM System. *European Journal of Electrical Engineering and Computer Science*, *2*. https://doi.org/10.24018/ejece.2018.2.7.44

Loke, M. (2001). Electrical imaging surveys for environmental and engineering studies. *A Practical Guide to 2D and 3D Surveys*.

Mitchell, M. A., & Oldenburg, D. W. (2023). Using DC resistivity ring array surveys to resolve conductive structures around tunnels or mine-workings. *Journal of Applied Geophysics*, 104949. https://doi.org/10.1016/j.jappgeo.2023.104949

Nassereddine, M., Rizk, J., & Nasserddine, G. (2013). Soil Resistivity Data Computations; Single and Two - Layer Soil Resistivity Structure and Its Implication on Earthing Design. *International Journal of Electrical and Computer Engineering*, *7*, 35–40.

Okpoli, C. C. (2013). Sensitivity and Resolution Capacity of Electrode Configurations. *International Journal of Geophysics*, *2013*, 1–12. https://doi.org/10.1155/2013/608037

Olayinka, A. I., & Yaramanci, U. (2000). Assessment of the reliability of 2D inversion of apparent resistivity data. *Geophysical Prospecting*, *48*(2), 293–316. https://doi.org/10.1046/j.1365-2478.2000.00173.x

Oyeyemi, K. D., Aizebeokhai, A. P., Metwaly, M., Omobulejo, O., Sanuade, O. A., & Okon, E. E. (2022). Assessing the suitable electrical resistivity

arrays for characterization of basement aquifers using numerical modeling. *Heliyon*, *8*(5), e09427. https://doi.org/https://doi.org/10.1016/j.heliyon.2022.e09427

Sirota, D., Shragge, J., Krahenbuhl, R., Swidinsky, A., Yalo, N., & Bradford, J. (2022). Development and validation of a low-cost direct current resistivity meter for humanitarian geophysics applications. *GEOPHYSICS*, *87*(1), WA1–WA14. https://doi.org/10.1190/geo2021-0058.1

Thapa, D. (2020). Use of two dimensional electrical resistivity tomography (2D-ERT) synthetic modelling to detect collapse masses. *Journal of Nepal Geological Society*, *60*, 139–145. https://doi.org/10.3126/jngs.v60i0.31250

Uhlemann, S., Chambers, J., Falck, W., Tirado Alonso, A., Fernández González, J., & Espín de Gea, A. (2018). Applying Electrical Resistivity Tomography in Ornamental Stone Mining: Challenges and Solutions. *Minerals*, *8*(11), 491. https://doi.org/10.3390/min8110491

Wróbel, M., Stan-Kłeczek, I., Marciniak, A., Majdański, M., Kowalczyk, S., Nawrot, A., & Cader, J. (2022). Integrated Geophysical Imaging and Remote Sensing for Enhancing Geological Interpretation of Landslides with Uncertainty Estimation—A Case Study from Cisiec, Poland. *Remote Sensing*, *15*(1), 238. https://doi.org/10.3390/rs15010238